PERIODICO di MINERALOGIA
established in 1930

Dipartimento
di Scienze della Terra
Sapienza
Università di Roma

An International Journal of
Mineralogy, Crystallography, Geochemistry,
Ore Deposits, Petrology, Volcanology
and applied topics on Environment, Archaeometry and Cultural Heritage

Evidence on the development of a wide high-T hydrothermal system in the Ischia volcanic field before Mt. Epomeo resurgence: new insights from investigation of hydrothermally altered lithic clasts of Secca d'Ischia volcanic deposits

Paolo Fulignati, Paola Marianelli *

Department of Earth Sciences, University of Pisa, 56126 Pisa, Italy

ARTICLE INFO

Submitted: October 2022
Accepted: November 2022
Available on line: December 2022

* Corresponding author:
paola.marianelli@unipi.it

Doi: 10.13133/2239-1002/17883

How to cite this article:
Fulginati P. and Marianelli P. (2022)
Period. Mineral. 91, 291-302

ABSTRACT

This work is focused on the hydrothermal system developed in the Ischia volcanic field before Mt. Epomeo resurgence, and is based on the investigation of hydrothermally altered lithic clasts present in the volcanic deposits of Secca d'Ischia and Epomeo Green Tuff eruptions. We demonstrate that a wide high temperature hydrothermal system occurred in the Ischia volcanic complex, both in intracalderic and extracalderic areas, at the time of the caldera-forming paroxysmal phase (60-56 ka). This hydrothermal system was characterized by high temperatures ranging from 240 °C and 340 °C and fluids of marine (~3.5 wt% $NaCl_{equiv.}$) and meteoric origin (<0.5 wt% $NaCl_{equiv.}$). In the intracalderic area, the hydrothermal system was exhumed during the resurgence of Mt. Epomeo; in the extracalderic area of the island the hydrothermal system was at least partially disrupted during the Secca d'Ischia eruption.

Keywords: Ischia Island; hydrothermal system; fluid inclusions; lithic clasts; Secca d'Ischia eruption.

INTRODUCTION

The volcanic field of Ischia is part of the wide and active Phlegraean Volcanic District (Orsi et al., 1996). Ischia volcanism develops between 150 ka and 1301-1302 AD (Sbrana et al., 2018 and reference therein) in both continental and marine environments (Passaro et al., 2016) and is made mainly by monogenetic volcanoes (tuff cones, scoria cones, spatter cones and spatter ramparts, lava domes and lava flows) dispersed over an area of 250 km^2. Volcanics have mainly trachytic compositions (Vezzoli, 1988), whereas trachybasalts and shoshonites characterize few deposits. Some paroxysmal eruptions, occurred between 60 and 56 ka, are linked to the Ischia caldera formation (Vezzoli, 1988; Carlino et al., 2006; Brown et al., 2008; Carlino, 2012; Sbrana et al., 2009, 2018), and at the end of the paroxysmal phase, a significant submarine volcano (Secca d'Ischia) formed in the south-eastern offshore (Figure 1) of the Ischia volcanic field (Sbrana et al., 2018), whose deposits occur on the southeastern hill of the island. The tuffaceous units ponded inside the caldera outcrop at present on Mt Epomeo, which represents the resurgence, attributable to a laccolite-shaped shallow magma body (Rittmann, 1930; Carlino et al., 2006; Sbrana et al., 2009; Carlino, 2012; Carlino et al., 2022 and references therein), of the central portion of the caldera (Orsi et al., 1991; Acocella and Funicello, 1999; Carlino et al., 2006; Sbrana et al., 2009, 2018). The starting of the resurgence occurred between the 56 ka caldera collapse and 33 ka, when the resurgent block was largely uplifted (Carlino et al., 2022).

Strong hydrothermal activity accompanied this volcanic phase, and the intracalderic area was characterized by the development of a high-temperature hydrothermal system (Sbrana et al., 2009), which is now partially exposed on the

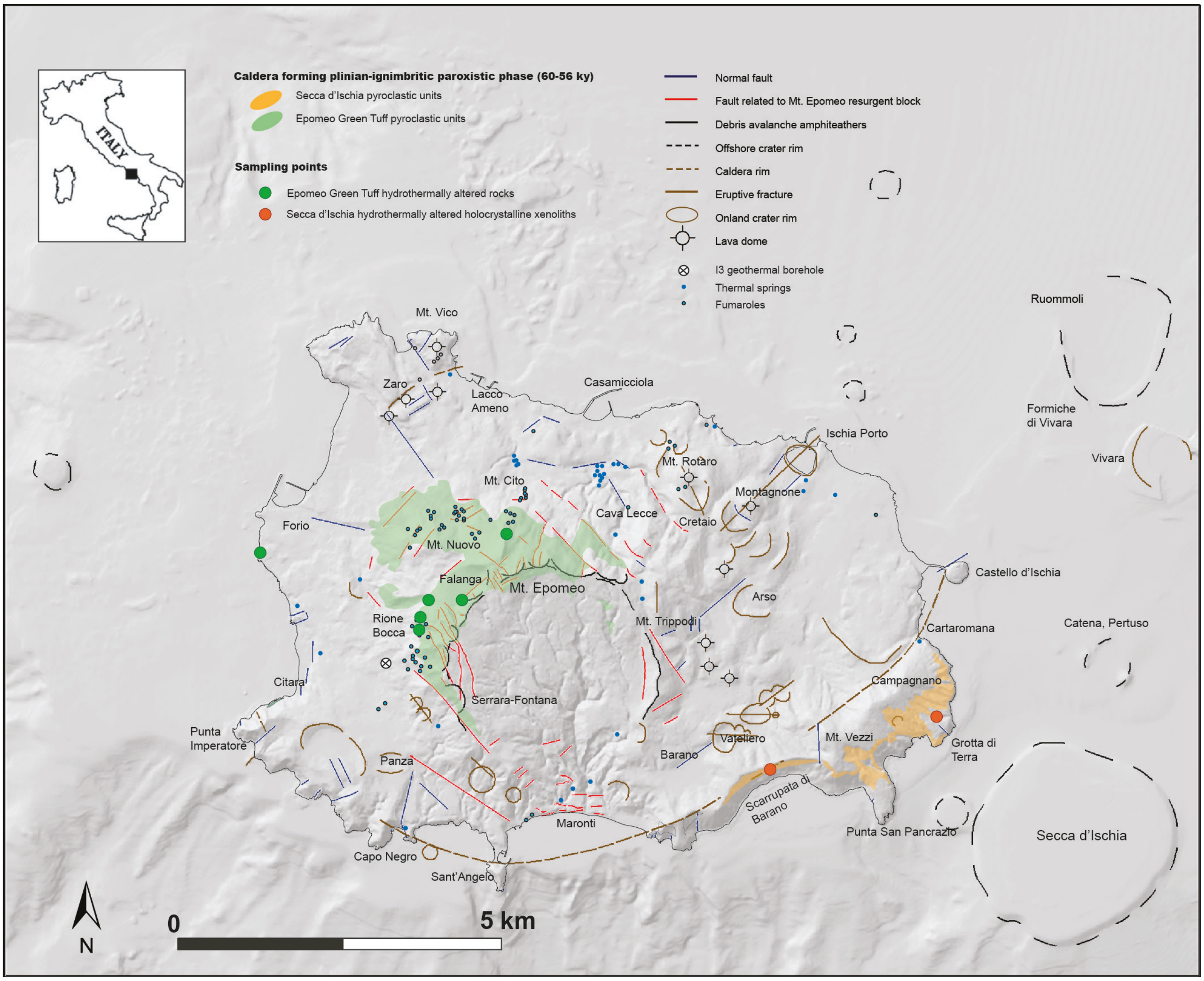

Figure 1. Structural sketch of the Ischia volcanic field (modified from Sbrana et al., 2018) with location of sampling points and of the main outcrops of Epomeo Green Tuff and Secca d'Ischia units.

flanks of the Mt. Epomeo resurgent block. The occurrence of hydrothermally altered lithic clasts in the deposits of Secca d'Ischia suggests that an intense hydrothermal activity was also peculiar of the extracalderic area of the volcanic field. The aim of this work is to investigate the characteristics of this hydrothermal system, disrupted during the Secca d'Ischia explosive activity, in the general framework concerning the significant hydrothermal activity that interested Ischia volcanic field before the resurgence of the Mt. Epomeo.

ANALYTICAL METHODS

Scanning-Electron-Microscope-Energy-Dispersive-System (SEM-EDS) microanalysis was carried out on individual minerals using a ThermoFisher Quanta 400 Forensic equipped with a Pathfinder microanalysis. Operating conditions were 20 kV and about 0.1 nA beam current. The analyses were normalized to 100 wt% due to the Pathfinder software used (Dipartimento di Scienze della Terra, University of Pisa). Analytical results, errors, reproducibility and detection limits using international standards for SEM-EDS technique are reported in Fulignati et al. (2019).

Petrography and microthermometric determinations of fluid inclusions (FIs) were carried out on double polished thin sections (100-300 µm thick). For the microthermometric experiments on fluid inclusions a Linkam THMS 600 heating/freezing stage was used. The accuracy of measurements was ±2 °C at 398 °C controlled by the melting point of $K_2Cr_2O_7$, ±0.1 °C at 0 °C and ±0.2

°C at -56.6 °C controlled by using certified pure water and CO_2-bearing synthetic fluid inclusions (Synthetic Fluid Inclusion Reference Set, Bubbles Inc., USA). The rate of heating and freezing experiments was varied as a function of the rate of transformations in the inclusions and ranged from 5 to 30 °C/min.

RESULTS

The studied lithic clasts were collected from Secca d'Ischia deposits and Epomeo Green Tuff (Figure 1). Secca d'Ischia samples come from a lithic-rich layer mainly formed by lava (76 wt%) and holocrystalline (20 wt%) lithic clasts. The latter are always covered by a reddish patina, which is a peculiar feature of this deposit (Figure 2). Lithic clasts from the Epomeo Green Tuff are found in the hydrothermally altered intracaldera tuffaceous units that constitute the succession of the uplifted block located at the caldera center (Sbrana et al., 2018). All the studied lithic clasts generally have a near holocrystalline texture and are interpreted to represent fragments of subvolcanic bodies. The primary mineralogical assemblage is formed by K-feldspar, plagioclase, clinopyroxene, biotite, minor amphibole and accessory apatite, titanite, monazite and thorite.

Most of the investigated subvolcanic lithic clasts show a widespread hydrothermal alteration and 16 were selected for detailed investigation. The hydrothermal alteration mineralogical paragenesis is dominated by the assemblage formed by albite + adularia + mixed layers chlorite/smectite (C/S)+ illite ± mixed layers biotite/vermiculite (B/V) ± chlorite (Figure 3).

Chemistry of hydrothermal minerals

Feldspars

Both plagioclase and K-feldspar show a nearly stoichiometric composition. The composition of K-feldspar shows very little substitution of Ab molecules for Or and negligible presence of Ca and Fe and can be considered adularia. Plagioclase composition involves only little amount of K (Table 1) and can be considered albite.

Chlorite and mixed layers C/S

The chemical composition indicated that most of the analyzed chlorites are not pure chlorite but mixed layers C/S. It is possible to distinguish the mixed layers C/S (Table 2) from pure chlorite for their greater number of interlayer cations (Na+K+Ca >0.10 cations/28 Ox) and for a greater amount of Si (IV) cations (>6.25 cations/28 Ox) (Bettison and Shiffman, 1988). The variable contents in silica, octahedral vacancy and large radii cations (Na-K-Ca) suggest that the content in smectite layers is quite variable in these mixed layers C/S (Table 2). When plotted in an Al (IV) vs total number of octahedral cations (formula recalculated on the basis of 25 Ox) diagram (Figure 4), mixed layers C/S approach the linear relation found for corrensite by Inoue (1995) and Inoue and Utada (1991). This may suggest that at least part of these mixed layers C/S are not randomly interstratified but regularly interstratified (corrensite). The compositional relationships between mixed layers C/S and chlorite can be viewed on an M^{+}-4Si-$3R^{2+}$ diagram (Figure 5), as proposed by Meunier et al. (1991). In this diagram, analyses of mixed layers C/S fall around the dashed line

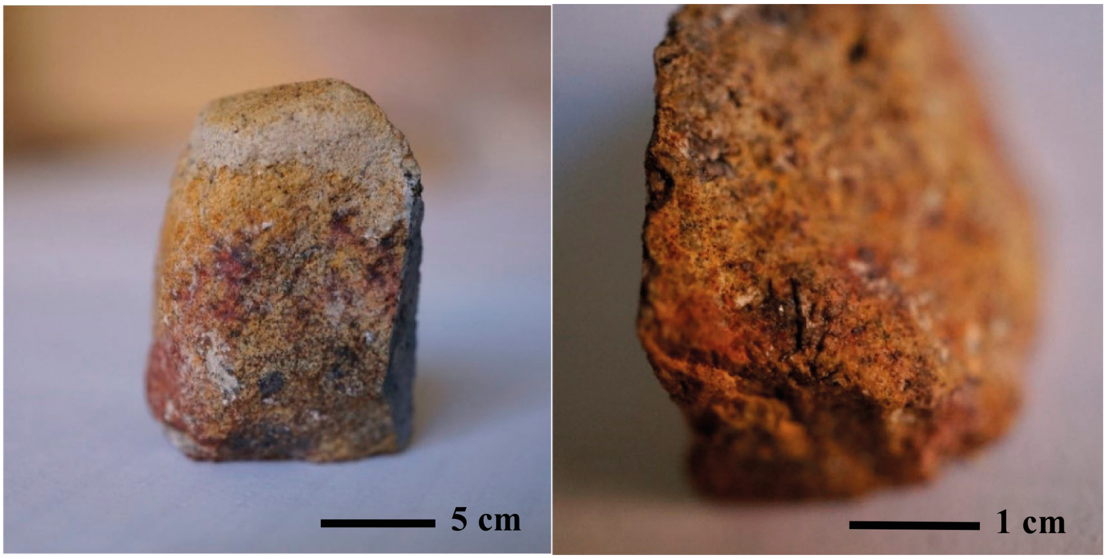

Figure 2. Pictures of hydrothermally altered holocrystalline lithic clast of the Secca d'Ischia deposits. Note the reddish patina that typically covers the clasts.

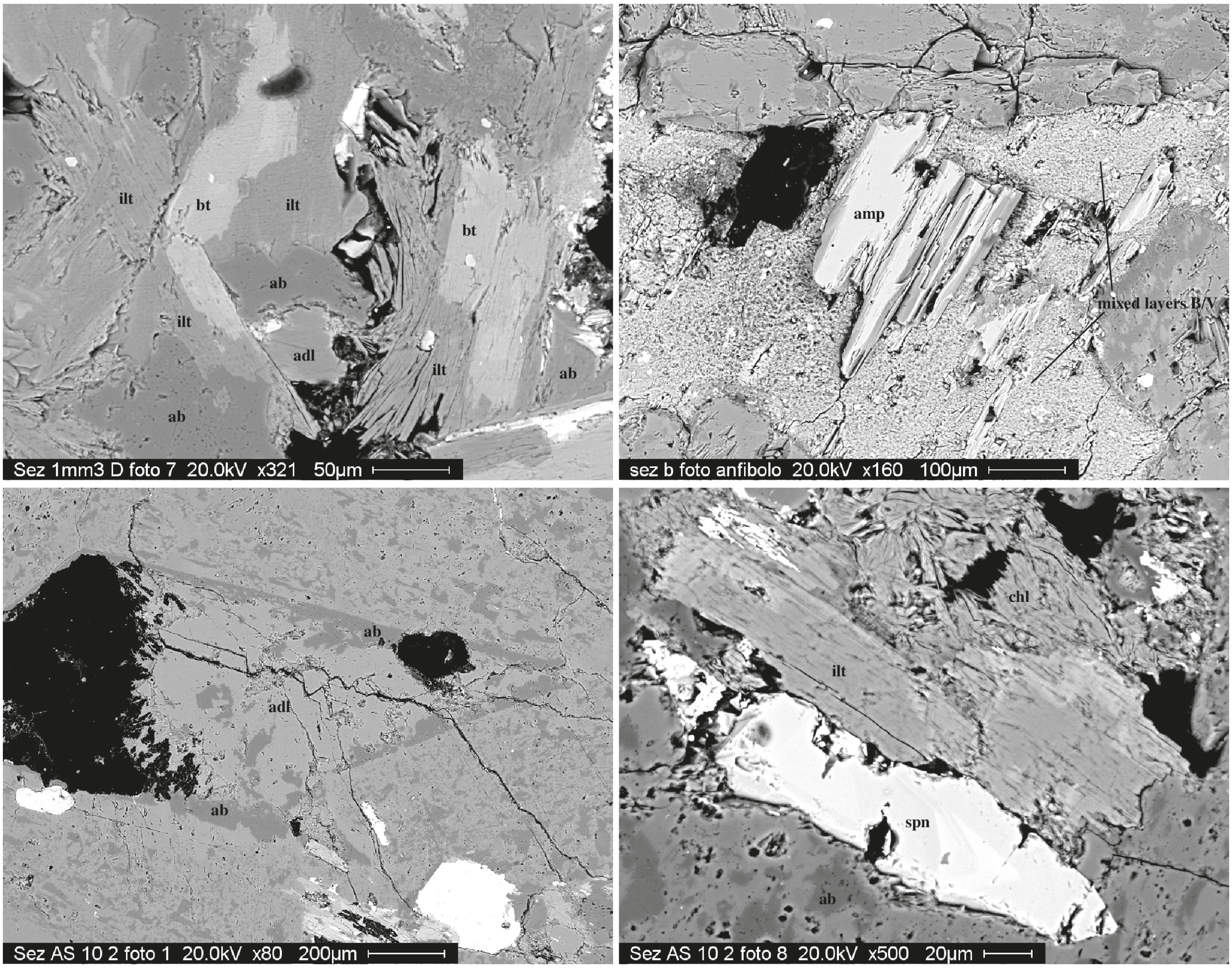

Figure 3. Scanning electron microscopy images. (a) Pervasive alteration, made up of adularia + albite + illite, obliterates the primary mineralogical assemblage of the lithic clast. Biotite is the only primary mineral that is still distinguishable. (b) Mixed layers biotite/vermiculite (B/V) partially overprinting primary amphibole. (c) Primary mineral (probably plagioclase) substituted by albite and adularia association. (d) Primary biotite altered by illite and chlorite. Abbreviations: bt = biotite, ilt = illite, ab = albite, adl = adularia, amp = amphibole, chl = chlorite, spn = sphene. Mineral abbreviations follow Whitney and Evans (2010).

Table 1. Representative analyses of authigenic albite and adularia.

	albite								adularia							
SiO_2	68.37	67.95	67.98	68.70	68.61	69.94	68.71	68.37	64.83	64.70	64.30	64.03	64.01	64.97	64.42	64.25
Al_2O_3	20.08	20.08	19.97	19.78	19.99	19.78	20.02	20.26	18.55	18.58	18.53	18.92	18.61	19.02	18.91	18.72
FeO	bdl	0.06	0.05	bdl	bdl	bdl	bdl	bdl	bdl	0.16	0.08	0.08	0.16	0.16	bdl	bdl
CaO	0.39	0.40	0.45	0.39	0.26	0.16	0.4	0.24	bdl	bdl	bdl	0.07	bdl	bdl	bdl	bdl
Na_2O	10.81	11.13	11.00	11.00	10.95	11.07	10.72	11.08	0.92	0.30	0.50	0.48	0.21	0.75	0.28	0.69
K_2O	0.35	0.38	0.54	0.13	0.19	0.05	0.14	0.05	15.70	16.25	16.38	16.03	17.02	15.94	16.39	16.34
An	1.92	1.91	2.14	1.91	1.28	0.79	2.00	1.18	0.00	0.00	0.00	0.35	0.00	0.00	0.00	0.00
Ab	96.04	95.94	94.80	97.34	97.61	98.92	97.16	98.53	8.18	2.73	4.42	4.31	1.84	7.48	2.53	6.03
Or	2.05	2.16	3.06	0.76	1.11	0.29	0.84	0.29	91.82	97.27	95.58	95.35	98.16	92.53	97.47	93.97

bdl= below detection limit; total iron as FeO.

Table 2. Representative analyes of authigenic chlorite and mixed layers C/S.

	chlorite	chlorite	chlorite	chlorite	C/S	C/S	C/S	C/S	C/S	C/S	C/S	C/S	C/S	C/S	C/S	C/S	C/S	C/S
SiO_2	33.18	31.32	31.62	33.96	37.73	38.13	43.02	41.01	39.82	37.51	37.33	36.37	37.74	41.08	44.39	38.43	40.75	36.43
TiO_2	bdl	bdl	bdl	bdl	bdl	bdl	bdl	bdl	bdl	bdl	bdl	bdl	0.46	0.60	0.84	1.05	1.06	1.14
Al_2O_3	19.8	21.20	20.73	22.72	18.20	18.39	15.12	14.35	16.05	18.13	17.72	18.20	17.99	18.67	14.35	18.88	18.76	18.34
FeO	26.71	27.72	27.55	21.78	21.93	21.14	16.06	15.99	20.59	21.25	22.61	23.67	25.31	20.98	24.74	22.95	21.72	25.85
MnO	1.39	1.90	1.69	1.10	1.02	0.77	0.54	2.81	1.13	1.13	1.10	1.38	0.95	0.91	0.56	bdl	bdl	bdl
MgO	18.54	17.41	18.14	20.12	19.87	20.12	22.19	22.33	18.63	20.29	18.86	18.37	16.26	15.91	12.75	17.45	16.56	17.22
CaO	0.21	0.08	0.13	0.22	0.19	0.27	0.66	0.96	0.72	0.48	0.51	0.32	0.43	0.37	0.63	0.22	0.53	0.36
Na_2O	bdl	0.16	bdl	bdl	0.17	0.17	0,24	bdl	0.22	0.17	0.09	bdl	bdl	bdl	0.29	bdl	bdl	bdl
K_2O	0.16	0.22	0.14	0.10	0.89	1.01	2.18	2.55	2.84	1.03	1.79	1.68	0.86	1.48	1.44	1.02	0.62	0.66
Total	99.99	100.01	100.00	100.00	100.00	100.00	100.01	100.00	100.00	99.99	100.01	99.99	100.00	100.00	99.99	100.00	100.00	100.00
Si	6.080	5.800	5.840	6.038	6.714	6.751	7.434	7.220	7.114	6.675	6.714	6.585	6.811	7.216	7.895	6.816	7.130	6.579
Al (IV)	1.920	2.200	2.160	1.962	1.286	1.249	0.566	0.780	0.886	1.325	1.286	1.415	1.189	0.784	0.105	1.184	0.870	1.421
Al (VI)	2.355	2.426	2.352	2.798	2.530	2.587	2.513	2.197	2.493	2.477	2.469	2.468	2.636	3.080	2.903	2.762	2.997	2.481
Ti	0.000	0.000	0.000	0.000	0.000	0.000	0.000	0.000	0.000	0.000	0.000	0.000	0.062	0.079	0.112	0.140	0.139	0.155
Fe	4.091	4.291	4.254	3.237	3.262	3.129	2.320	2.353	3.075	3.161	3.399	3.583	3.818	3.080	3.678	3.402	3.177	3.902
Mn	0.216	0.298	0.264	0.166	0.154	0.115	0.079	0.419	0.171	0.170	0.167	0.212	0.145	0.135	0.084	0.000	0.000	0.000
Mg	5.061	4.802	4.991	5.329	5.267	5.306	5.712	5.856	4.958	5.378	5.053	4.955	4.371	4.163	3.378	4.610	4.316	4.632
Ca	0.041	0.016	0.026	0.042	0.036	0.051	0.122	0.181	0.138	0.091	0.098	0.062	0.083	0.070	0.120	0.042	0.099	0.070
Na	0.000	0.057	0.000	0.000	0.059	0.058	0.080	0.000	0.076	0.059	0.031	0.000	0.000	0.000	0.100	0.000	0.000	0.000
K	0.037	0.052	0.033	0.023	0.202	0.228	0.480	0.572	0.647	0.234	0.411	0.388	0.198	0.331	0.327	0.231	0.138	0.152
Fe/(Fe+Mg)	0.447	0.472	0.460	0.378	0.382	0.371	0.289	0.287	0.383	0.370	0.402	0.420	0.466	0.425	0.521	0.425	0.424	0.457
oct. vacancy	0.277	0.183	0.139	0.471	0.788	0.863	1.376	1.175	1.303	0.814	0.911	0.783	0.968	1.462	1.845	1.086	1.371	0.830

bdl = below detection limit. Chlorite and mixed layers C/S analyses calculated on the basis of 28 oxygens. Total iron as FeO.

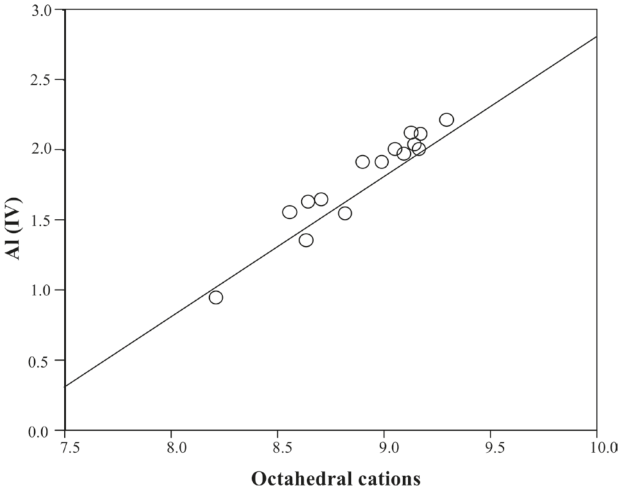

Figure 4. Al (IV) vs total octahedral cations (25 ox) diagram for mixed layers C/S. The solid line represents the linear relation found for corrensite by Inoue (1995) and Inoue and Utada (1991).

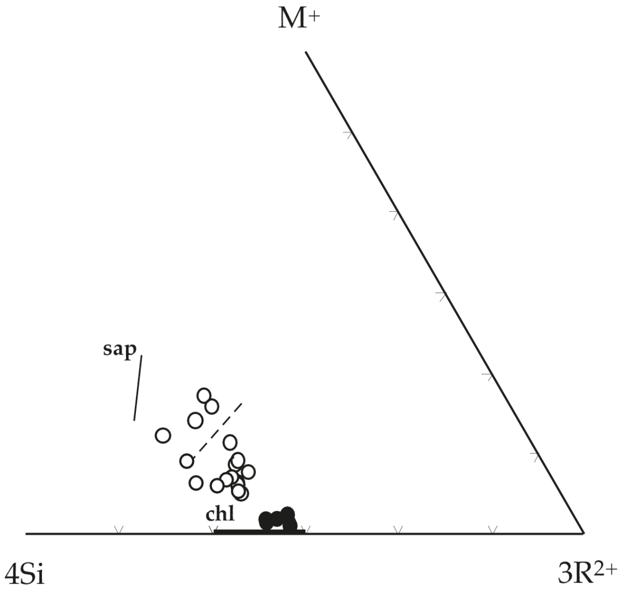

Figure 5. Mixed layers C/S and chlorite analyses plotted on a M+-4Si-3R2+ diagram (Meunier et al. 1991). The theoretical 50-50 corrensite composition is given by the dashed line. Open dots = mixed layers C/S; black dots = chlorite.

representing the ideal 50-50 corrensite composition, and depict a trend towards the chlorite pure term, with several analyses that fall well below the dashed line (Figure 5). We may consider these latter analyses as representative of mixtures of corrensite with a discrete chlorite (Meunier et al., 1991). This indicates that these mixed layers C/S have a high chlorite content, as confirmed by Figure 6 diagram in which these analyses fall very close to the chlorite end-member. The high chlorite content suggests relatively high equilibrium crystallization temperature, compatible with propylitic alteration facies, according to Tomasson and Kristmannsdottir (1972), Schiffman and Fridleiffson (1991), Inoue and Utada (1991), Schiffman and Staudigel (1995), Robinson and Zamora (1999).

Mixed layers B/V

Mixed layers B/V (Table 3) were found in some samples as alteration of K-feldspar and amphibole. Microanalytical data show a negative linear correlation of Ca with K (Figure 7a), whereas (Fe+Mg) has an almost constant value with varying K (Figure 7b). This suggests that Ca is the dominant interlayer cation, while Mg occurs only in small quantities, in the vermiculite layers, (Mc Dowell and Elders, 1980). The occurrence of mixed layers B/V is consistent with the development of propylitic alteration facies as indicated by McDowell and Elders (1980) and Fulignati et al. (1997).

Illite

Illite (Table 4), often associated with albite, is mainly found as alteration of primary K-feldspar and sometimes in veinlets. It appears well crystalline and the analyses reveal an almost total filling of the interlayer site, suggesting a high temperature of formation (Bishop and Bird, 1987; Cathelineau, 1988).

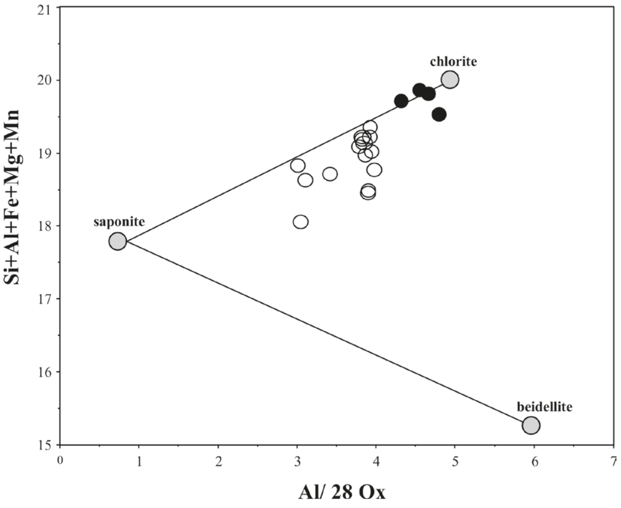

Figure 6. Sum of the major non interlayer cations (Si+Al+Fe+Mg) versus Al diagram (Schiffman and Fridleifsson, 1991) for mixed layers C/S and chlorite, where we can represent the compositional differences between smectite, chlorite and their interlayer terms. All analyses are recalculated on the basis of 28 oxygens. Open dots = mixed layers C/S; black dots = chlorite.

Table 3. Representative analyes of mixed layers biotite/vermiculite.

SiO_2	46.18	46.65	40.57	48.04	46.67
TiO_2	0.07	bdl	bdl	0.22	0.09
Al_2O_3	15.47	15.85	13.60	14.16	15.50
FeO	20.00	19.74	19.91	18.95	6.82
MnO	1.15	1.40	8.57	0.95	0.16
MgO	9.92	9.66	10.39	11.83	23.92
CaO	0.89	0.87	2.41	1.88	2.97
Na_2O	0.82	0.47	0.29	0.40	1.70
K_2O	5.51	5.35	4.26	3.56	2.17
Total	100.00	100.00	100.00	100.00	100.00
Si	6.449	6.488	5.945	6.590	6.092
Al (IV)	1.551	1.512	2.055	1.410	1.908
Al (VI)	0.995	1.085	0.293	0.879	0.476
Ti	0.007	0.000	0.000	0.023	0.009
Fe	2.335	2.295	2.439	2.173	0.744
Mn	0.136	0.165	1.063	0.110	0.018
Mg	2.064	2.001	2.268	2.417	4.651
Ca	0.133	0.130	0.378	0.276	0.415
Na	0.222	0.127	0.082	0.106	0.430
K	0.981	0.949	0.796	0.623	0.361

bdl = below detection limit.

Chlorite and Illite geothermometers

Chlorite composition can be used to estimate formation temperature, using the empirical geothermometers of Cathelineau (1988), Kranidiotis and McLean (1987) and Jowett (1991) that are based on the observed systematic increase of Al (IV) content of chlorite with increasing temperature of formation. The average temperatures calculated with different geothermometers are between 250° and 300 °C (Table 5).

Formation temperature of illite was estimated using the Bishop and Bird (1987) geothermometer, based on the temperature-dependent relationships of a_{pyr} and a_{musc} in illite (log a_{pyr} and log a_{musc} in illite decrease systematically with increasing temperature), and the geothermometer proposed by Battaglia (2004). The average temperature, calculated with log(a_{pyr})-T and log(a_{musc})-T relations, gave a range of 265°-300 °C and 300 °C- 330 °C respectively, that calculated with Battaglia (2004) geothermometer gave similar values ranging between 265 °C and 315 °C (Table 5).

Fluid inclusion analysis

Fluid inclusions were found within primary K-feldspar crystals of hydrothermally altered Epomeo Green Tuff subvolcanic lithic clasts, whereas in those of Secca d'Ischia FIs were not observed. All descriptions refer to fluid inclusion assemblages (FIAs, Goldstein and Reynolds, 1994). The observed inclusions occur as trails that crosscut the K-feldspar crystals (Figure 8a) suggesting a secondary origin according to the criteria of Roedder (1984) and Goldstein (2003). Microscopic observation at room temperature revealed the occurrence of one main type of FIs in the examined samples (Type 1). These FIs are two-phase liquid-rich (L+V), are small in size (5-15

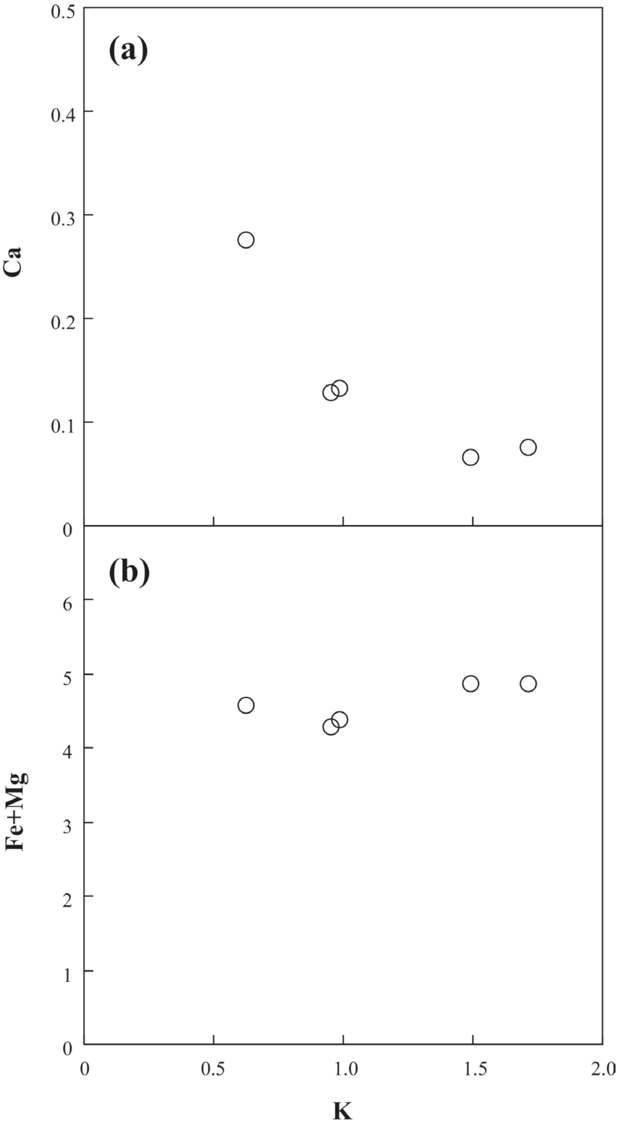

Figure 7. Ca vs K (a) and Fe+Mg vs K (b) diagrams for mixed layers B/V.

Table 4. Representative analyes of authigenic illite.

SiO_2	46.44	47.67	49.51	49.69	50.79	46.98	50.41	49.00	47.88	45.75
TiO_2	bdl	0.27	0.09	bdl	0.09	bdl	bdl	bdl	bdl	bdl
Al_2O_3	36.58	37.89	35.12	35.57	35.53	37.50	32.27	38.77	39.61	37.13
FeO	4.17	1.52	3.75	269	1.65	2.80	3.32	0.80	0.72	2.49
MnO	bdl	bdl	bdl	bdl	bdl	bdl	bdl	bdl	0.17	0.40
MgO	1.24	0.33	0.41	0.94	1.00	0.61	1.47	0.54	0.55	1.94
CaO	bdl	0.06	bdl	bdl	bdl	bdl	bdl	bdl	bdl	0.16
Na_2O	0.51	0.09	bdl	bdl	0.10	0.26	bdl	bdl	bdl	bdl
K_2O	11.06	12.07	11.12	11.11	10.83	11.85	12.52	10.89	11.08	12.13
Total	100.00	100.00	100.00	100.00	100.00	100.00	100.00	100.00	100.00	100.00
Si	2.988	3.043	3.165	3.160	3.204	3.017	3.246	3.081	3.020	2.954
Al (IV)	1.002	0.957	0.835	0.840	0.796	0.983	0.754	0.919	0.980	1.046
Al (VI)	1.780	1.893	1.811	1.825	1.845	1.854	1.695	1.954	1.964	1.780
Ti	0.000	0.013	0.004	0.000	0.004	0.000	0.000	0.000	0.000	0.000
Fe	0.225	0.081	0.200	0.143	0.087	0.150	0.179	0.042	0.038	0.134
Mn	0.000	0.000	0.000	0.000	0.000	0.000	0.000	0.000	0.009	0.022
Mg	0.119	0.031	0.039	0.089	0.094	0.058	0.141	0.051	0.052	0.187
Ca	0.000	0.004	0.000	0.000	0.00	0.000	0.000	0.000	0.000	0.011
Na	0.064	0.011	0.000	0.000	0.012	0.032	0.000	0.000	0.000	0.000
K	0.910	0.982	0.907	0.901	0.871	0.970	1.028	0.873	0.891	0.999

bdl = below detection limit. Illite analyses calculated on the basis of 11 oxygens. Total iron as FeO.

Table 5. Temperatures calculated from chlorite and illite geothermometers.

chlorite geothermometers	
K&ML87	254-285
C88	247-292
J91	251-297
illite geothermometers	
B&B87 (apyr)	265-301
B&B87 (amusc)	300-330
B04	265-315

Temperatures are expressed in °C. K&ML87 (Kranidiotis and McLean, 1987); C88 (Cathelineau, 1988); J91 (Jowett, 1991); B&B (Bishop and Bird, 1987); B04 (Battaglia 2004).

μm) and generally show an irregular shape (Figure 8b). They are characterized by a scarce variability in the vapor/liquid ratio, with the vapor bubble that occupies around 20-25% of the total volume of the inclusions.

Results of microthermometric analysis are reported in Figure 9 a,b. During cooling experiments, FIs freeze to ice below -25/-30 °C, as observed by the sudden shrinkage of the vapor bubble. Upon warming, FIs exhibit a temperature of first ice melting (T_e) around -21/-22 °C suggesting that Na^+ is the predominant cation in solution (eutectic of H_2O-NaCl system is -20.8/-21.2 °C; Crawford, 1981). The temperature of final ice melting (T_{mi}) ranges from -0.1 °C to -1.4 °C with a mode at -0.2 °C. This corresponds to salinities ranging between 0.2 and 2.4 wt% $NaCl_{equiv.}$ with a mode around 0.3 wt% $NaCl_{equiv.,}$ as calculated according to Bodnar (1993). During heating experiments the total homogenization (T_h) occurs by bubble disappearance at a temperature in the range 249-312 °C with a mode at about 265 °C.

Discussion

The study of lithic clasts in deposits of volcanic eruptions represents a very useful tool for the investigation of magmatic-hydrothermal processes occurring at the peripheral portions of active magma chambers. Indeed, cognate lithics can be seen as frozen snapshots of the magma chamber-wall rock interface, captured at the

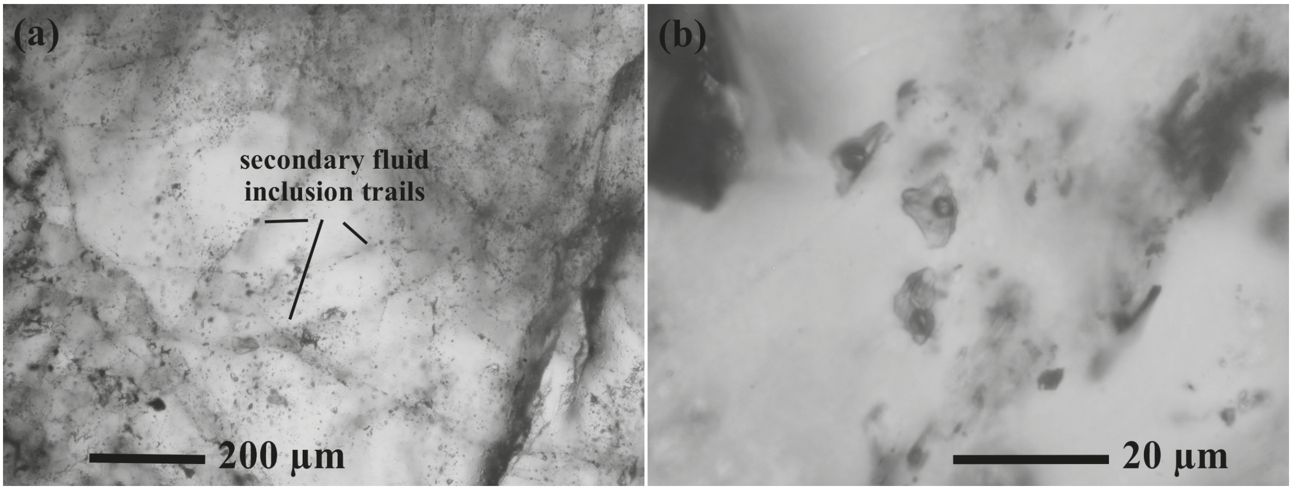

Figure 8. Microphotographs of fluid inclusions. (a) Secondary trails of Type 1 liquid-rich (L+V) fluid inclusions; (b) Type 1 liquid-rich (L+V) fluid inclusions.

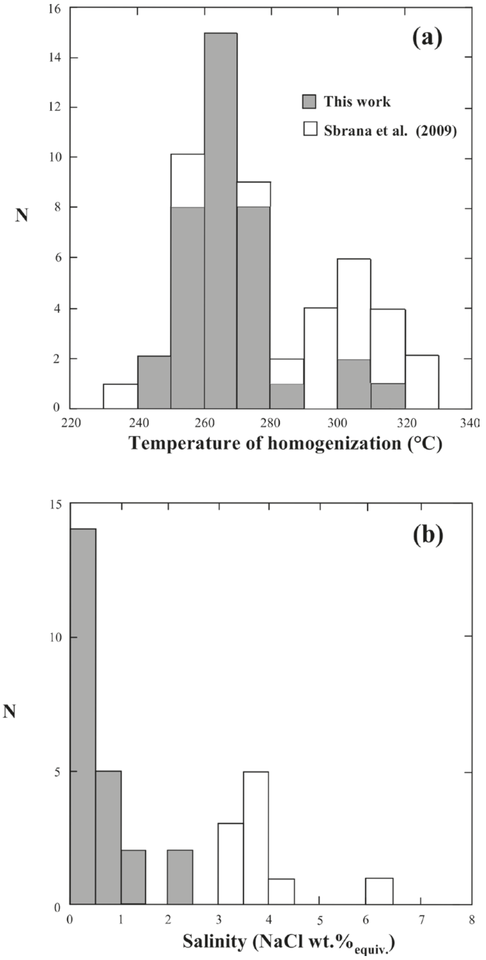

Figure 9. Histograms of the homogenization temperatures (a) and salinities (b) of the studied fluid inclusions. Data from Sbrana et al. (2009) are reported for comparison. N=number of measurements.

moment of the eruption that disrupted the chamber itself (Matthews et al., 1996; Del Moro et al., 2001; Fulignati et al., 2001, 2004 a,b, 2005, 2011; Gilg et al., 2001; Sbrana et al., 2009).

The study of hydrothermally altered lithic clasts of Secca d'Ischia deposits revealed the existence of a hydrothermal system that was active in the area before the eruption. This is evidenced by the pervasive hydrothermal alteration that affects most of the studied lithics and by the secondary mineralogical assemblage, which is typical of a propylitic alteration zone. The application of mineralogical geothermometers to minerals (illite, chlorite) of the alteration paragenesis suggests that this was a high-temperature hydrothermal system, characterized by fluid temperatures ranging between about 250 °C and 300 °C (Table 5), which well agree with a propylitic alteration facies. The magmatic system involved in the Secca d'Ischia eruption should have represented the engine that generated the thermal anomaly of the area. During the first phases of the eruption, at least part of the hydrothermal system was disrupted, and its wrenched portions occur as lithic clasts mainly concentrated in the reddish lithic-rich layer of Secca d'Ischia deposits outcropping on Ischia Island. High-temperature hydrothermal circulation characterized also the present intracalderic area of Ischia Island. This hydrothermal system affected both tuffaceous deposits, filling caldera depression, following the paroxysmal, caldera-forming phase (about 60 ka), and the subvolcanic bodies present in the deeper parts of the island to a depth of at least 1 km (Sbrana et al., 2009; Carlino et al., 2022). Fluid inclusions and mineralogical data indicate the existence of a complex hydrothermal system where fluids of marine and meteoric origin occurred (Figure 10). Indeed, the low salinity value of the fluid inclusions studied in this work (Figures 9 and 10) indicates that a diluted fluid of meteoric origin was also involved in the hydrothermal system. The estimated temperatures of the hydrothermal fluids in the intracalderic area span from 240 and 340 °C, with the highest values only found in the hydrothermally altered deep syenite clasts of Epomeo Green Tuff. The occurrence of an active and complex hydrothermal circulation carried out by fluids having similar characteristics was reported by works on fumarolic fluids (Panichi et al., 1992; Di Napoli et al., 2009). Moreover, deep geothermal wells drilled between 1939 and 1955 in the western sector of the island found hydrothermal fluids with temperature around 250 °C (Penta, 1954). The occurrence of a magmatic hypersaline aqueous fluid phase, exsolved from Ischia magmatic system, was highlighted by Sbrana et al. (2009); and the formation of magmatic Na-rich fluids, as a consequence of deep degassing processes, has been also experimentally demonstrated by Perinelli et al. (2019). However, our data exclude the involvement of these magmatic fluids in the hydrothermal system occurred in the Ischia volcanic complex at the time of the caldera-forming paroxysmal phase.

This work highlights that a well-developed and widespread high-temperature hydrothermal system was active already before 60 ka in the Ischia volcanic field. In the intracalderic area, the hydrothermal system was exhumed during the resurgence of Mt. Epomeo block, linked to the intrusion of a laccolith-shaped shallow magma body (Sbrana et al., 2009; Carlino, 2012). Intense hydrothermal activity characterized also extracalderic area of the island (Secca d'Ischia), with estimated fluid temperatures comparable to those of the intracalderic area. Hydrothermal activity with similar characteristics is still active, particularly in the western sector of Ischia Island.

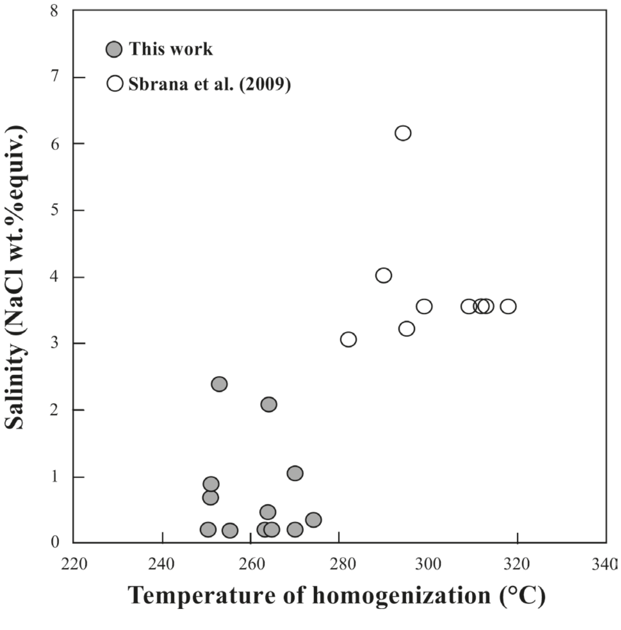

Figure 10. Salinity vs temperature of homogenization diagram for the studied fluid inclusions. Data from Sbrana et al. (2009) are reported for comparison. N=number of measurements.

CONCLUSIONS

This work testifies that a wide high-temperature hydrothermal system occurred in the Ischia volcanic complex at the time of the caldera-forming paroxysmal phase (60-56 ka). This was characterized by temperatures ranging from 240 °C and 340 °C and fluids of marine (~3.5 wt% $NaCl_{equiv.}$) and meteoric origin (<0.5 wt% $NaCl_{equiv.}$). These features are similar to the physico-chemical conditions characterizing the present active hydrothermal system on Ischia Island. Intense hydrothermal activity was present not only in the intracalderic area but also outside the caldera, particularly in the Secca d'Ischia zone.

The hydrothermal system, at least in its south-eastern extra-caldera portion, was disrupted after the onset of the Secca d'Ischia eruption. The occurrence of a developed high-temperature hydrothermal system in this area may have had important implications as concerns the eruptive dynamics of this volcanic event. We argue that the opening of the system may have in fact induced the decompression and flashing of the hydrothermal fluids, thus enhancing the explosivity of a phreatomagmatic eruptive phase.

ACKNOWLEDGEMENTS

This work is supported by the Università di Pisa under the "PRA Progetti di Ricerca di Ateneo" (Institutional Research Grants) Project no. PRA_2022-2023_66 "Fluid migration in the upper crust: from natural hazards to geo-resources". We are grateful to Mario Gaeta and Danilo M. Palladino for their comments and suggestions that help to improve the quality of the manuscript.

REFERENCES

Acocella V. and Funiciello R., 1999. The interaction between regional and local tectonics during resurgent doming: the case of the island of Ischia, Italy. Journal of Volcanology and Geothermal Research 88, 109-123.

Battaglia S., 2004. Variations in the chemical composition of illite from five geothermal fields: a possible geothermometer. Clay Minerals 39, 501-510.

Bettison L.A. and Schiffman P., 1988. Compositional and structural variations of phyllosilicates from the Point Sal Ophiolite, California. American Mineralogist 73, 62-76.

Bishop B.P. and Bird D.K., 1987. Variation in sericite compositions from fracture zones within the Coso Hot

Springs geothermal system, Geochimica et Cosmochimica Acta 51, 1245-1256.

Bodnar R.J., 1993. Revised equation and table for determining the freezing point depression of H_2O-NaCl solutions. Geochimica et Cosmochimica Acta 57, 683-684.

Brown R.J., Orsi G., De Vita S., 2008. New insights into Late Pleistocene explosive volcanic activity and caldera formation on Ischia (southern Italy). Bullettin of Volcanology 70, 583-603.

Carlino S., 2012. The process of resurgence for Ischia Island (southern Italy) since 55 ka: the laccolith model and implications for eruption forecasting. Bulletin of Volcanology 74, 947-961.

Carlino S., Cubellis E., Luongo G., Obrizzo F., 2006. On the mechanics of caldera resurgence of Ischia Island (southern Italy). In: Troise, C., De Natale, G., Kilburn, C.R.J. (Eds.), Mechanisms of Activity and Unrest at Large Calderas: Geol. Soc. London Sp. Publ., 269, pp. 181-193.

Carlino S., Sbrana A., Pino N.A., Marianelli P., Pasquini G., De Martino P., De Novellis V., 2022. The volcano-tectonics of the northern sector of Ischia Island caldera (Southern Italy): resurgence, subsidence and earthquakes. Frontiers in Earth Science 10, 730023.

Cathelineau M., 1988. Cation site occupancy in chlorites and illites as a function of temperature. Clay Minerals 23, 471-485.

Crawford M.L., 1981. Phase equilibria in aqueous fluid inclusions. In: L.S. Hollister and M.L. Crawford (Eds.), Short Course in Fluid Inclusions: Application to Petrology. Mineralogical Association of Canada 6, 75-100.

Del Moro A., Fulignati P., Marianelli P., Sbrana A., 2001. Magma contamination by direct wall rock interaction: constraints from xenoliths from the walls of a carbonate-hosted magma chamber (Vesuvius 1944 eruption). Journal of Volcanology and Geothermal Research 112, 15-24.

Di Napoli R., Aiuppa A., Bellomo S., Brusca L., D’Alessandro W., Gagliano Candela E., Longo M., Pecoraino G., Valenza M., 2009. A model for Ischia hydrothermal system: Evidences from the chemistry of thermal groundwaters, Journal of Volcanology and Geothermal Research 186, 133-159.

Fulignati P., Malfitano G., Sbrana A., 1997. The Pantelleria caldera geothermal system: data from the hydrothermal minerals. Journal of Volcanology and Geothermal Research 75, 251-270.

Fulignati P., Kamenetsky V.S., Marianelli P., Sbrana A., Mernagh T.P., 2001. Melt inclusion record of immiscibility between silicate, hydrosaline, and carbonate melts: application to skarn genesis at Mount Vesuvius. Geology 29, 1043-1046.

Fulignati P., Marianelli P., Proto M., Sbrana A., 2004a. Evidences of disruption of a magma chamber crystallizing front during caldera collapse: an example from the Breccia Museo unit (Ignimbrite Campana eruption). Journal of Volcanology and Geothermal Research 133, 141-155.

Fulignati P., Marianelli P., Santacroce R., Sbrana A., 2004b. Probing the Vesuvius magma chamber-host rock interface through xenoliths. Geological Magazine 4, 417-428.

Fulignati P., Kamenetsky V.S., Marianelli P., Sbrana A., 2005. Fluid inclusion evidence of second immiscibility within magmatic fluids (79 AD eruption of Mt. Vesuvius). Periodico di Mineralogia 74, 43-54.

Fulignati P., Kamenetsky V.S., Marianelli P., Sbrana A., Meffre S., 2011. First insights on the metallogenic signature of magmatic fluids exsolved from the active magma chamber of Vesuvius (AD 79 Pompei eruption). Journal of Volcanology and Geothermal Research 200, 223-234.

Fulignati P., Marianelli P., Sbrana A., 2019. Quantitative SEM-EDS analysis of reference silicate mineral and glass samples. Atti della Società Toscana di Scienze Naturali Serie A 126, 41-48.

Gilg H.A., Lima A., Somma R., Belkin H.E., De Vivo B., Ayuso R.A., 2001. Isotope geochemistry and fluid inclusion study of skarns from Vesuvius. Mineralogy and Petrology 73, 145-176.

Goldstein R.H., 2003. Petrographic analysis of fluid inclusions. in: Fluid Inclusions Analysis and Interpretation (I. Samson, A. Anderson and D. Marshall, editors). Mineralogical Association of Canada, Short Course Handbook, 32. Mineralogical Association of Canada, Quebec, Canada, 9-53

Goldstein R.H. and Reynolds T.J., 1994. Systematics of fluid inclusions in diagenetic minerals. Society for Sedimentary Geology Short Course 31, 1-199.

Inoue A., 1995. Formation of Clay Minerals in Hydrothermal Environments. In: Velde B. (Eds.) Origin and Mineralogy of Clays. Springer, Berlin, Heidelberg.

Inoue A. and Utada M., 1991. Smectite-to-chlorite transformation in thermally metamorphosed volcanoclastic rocks in the Kamikita area, northern Honshu, Japan. American Mineralogist 76, 628-640.

Jowett E.C., 1991. Fitting iron and magnesium into the hydrothermal chlorite geothermometer GACIMACISEG Joint Annual Meeting, p. 16 A62, Toronto, 27-29 May.

Kranidiotis P. and MacLean W.H., 1987. Systematics of chlorite alteration at the Phelps Dodge massive sulfide deposit, Matagami, Quebec Economic Geology 82, 1898-1911.

Matthews S.J., Marquillas R.A., Kemp A.J., Grange F.K., Gardeweg M.C., 1996. Active skarn formation beneath Lascar Volcano, northern Chile: a petrographic and geochemical study of xenoliths in eruption products. Journal of Metamorphic Geology 14, 509-530.

McDowell S.D. and Elders W.A., 1980. Authigenic layer silicate minerals in borehole Elmore 1, Salton Sea Geothermal Field, California, USA. Contribution to Mineralogy and Petrology 74, 293-310.

Meunier A., Inoue A., Beaufort D., 1991. Chemiographic Analysis of Trioctahedral Smectite-to-Chlorite Conversion Series from the Ohyu Caldera, Japan. Clays and Clay Minerals 39, 409-419.

Orsi G., Gallo G., Zanchi A., 1991. Simple-shearing block resurgence in caldera depressions. A model from Pantelleria and Ischia. Journal of Volcanology and Geothermal Research, 47, 1-11.

Orsi G., De Vita S., Di Vito, M., 1996. The restless, resurgent Campi Flegrei nested caldera (Italy): Constraints on its evolution and configuration. Journal of Volcanology and Geothermal Research, 74, 179-214.

Panichi C., Bolognesi L., Ghiara M.R., Noto P., Stanzione D., 1992. Geothermal assessment of the island of Ischia (southern Italy) from isotopic and chemical composition of the delivered fluids. Journal of Volcanology and Geothermal Research 49, 329-348.

Passaro S., De Alteriis G., Sacchi M., 2016. Bathymetric map of Ischia Island and its offshore (Napoli Bay, Italy). Journal of Maps 12, 152-159.

Penta F., 1954. Ricerche e studi sui fenomeni esalativo-idrotermali e il problema delle "forze endogene". Annali di Geofisica 8, 317-408.

Perinelli C., Gaeta M., Bonechi B., Granati S.F., Freda C., D'Antonio M., Stagno V., Sicola S., Romano C., 2019. Effect of water on the phase relations of primitive K-basalts: Implications for high-pressure differentiation in the Phlegraean Volcanic District magmatic system. Lithos 342-343, 530-541.

Rittmann A., 1930. Geologie der insel Ischia. Zeitschrift fur vulkanologie. Berlin. VI, pp. 268.

Robinson D. and Zamora A., 1999. The smectite to chlorite transition in the Chipilapa geothermal system, El Salvador. American Mineralogist 84, 607-619.

Roedder E., 1984. Fluid inclusions. Reviews in Mineralogy 12, pp. 646.

Sbrana A., Fulignati P., Marianelli P., Boyce A.J., Cecchetti A. 2009. Exhumation of an active magmatic-hydrothermal system in a resurgent caldera environment. The example of Ischia Island (Italy). Journal of the Geological Society of London 166, 1061-1073.

Sbrana A., Marianelli P., Pasquini G., 2018. Volcanology of Ischia (Italy). Journal of Maps 14, 494-503.

Schiffman P. and Fridleifsson G.O., 1991. The smectite–chlorite transition in drillhole NJ-15, Nesjavellir geothermal field, Iceland: XRD, BSE and electron microprobe investigations. Journal of Metamorphic Geology 9, 679-696.

Schiffman P. and Staudigel H., 1995. The smectite to chlorite transition in a fossil seamount hydrothermal system: the Basement Complex of La Palma, Canary Islands. Journal of Metamorphic Geology 13, 487-498.

Tomasson J. and Kristmannsdottir H., 1972. High temperature alteration minerals and thermal brines, Reykjanes, Iceland. Contribution to Mineralogy and Petrology 36, 123-134.

Vezzoli L., 1988. Island of Ischia. Quaderni de "La Ricerca Scientifica" progetto finalizzato "Geodinamica". Monografie finali 10, 134 pp.

Whitney D.L. and Evans B.W., 2010. Abbreviations for names of rock-forming minerals. Am. Mineral. 95, 185-187.